MEASUREMENT OF WETTED AREA FRACTION IN SUBCOOLED POOL BOILING OF WATER USING INFRARED THERMOGRAPHY

Hyungdae Kim[1,2], Youngjae Park[2], Jacopo Buongiorno[1,*]
[1] Massachusetts Institute of Technology, Cambridge, Massachusetts, USA
[2] Kyung Hee University, Youngin, Gyeonggi 446-701, Republic of Korea,
hdkims@khu.ac.kr, jacopo@mit.edu

Abstract

The wetted area fraction in subcooled pool boiling of water at atmospheric pressure is measured using the DEPIcT (DEtection of Phase by Infrared Thermography) technique. DEPIcT exploits the contrast in infrared (IR) light emissions between wet and dry areas on the surface of an IR-transparent heater to visualize the instantaneous distribution of the liquid and gas phases in contact with the heater surface. In this paper time-averaged wetted area fraction data in nucleate boiling are reported as functions of heat flux (from 30% up to 100% of the Critical Heat Flux) and subcooling (ΔT_{sub} = 0, 5, 10, 30 and 50°C). The results show that the wetted area fraction monotonically decreases with increasing heat flux and increases with increasing subcooling: both trends are expected. The range of time-averaged wetted area fractions is from 90%, at low heat flux and high subcooling, to 50% at high heat flux (right before CHF) and low subcooling. It is also shown that the dry areas are periodically rewetted by liquid sloshing on the surface at any subcooling and heat flux; however, the dry areas expand irreversibly at CHF.

Keywords: micro-hydrodynamics, CHF, DEPIcT

* Corresponding author

1. Introduction

Complex two-phase heat transfer phenomena such as nucleate boiling, critical heat flux, quenching and condensation govern the thermal performance of Light Water Reactors (LWRs) under normal operation and during transients/accidents. These phenomena are typically characterized by the presence of a liquid-vapor-solid contact line on the surface from/to which the heat is transferred. For example, in nucleate boiling, a significant fraction of the energy needed for bubble growth comes from evaporation of a liquid meniscus, or microlayer, underneath the bubble itself. As the liquid-vapor-solid line at the edge of the meniscus retreats, a circular dry patch in the middle of the bubble is exposed; the speed of the triple line retreat is one measure of the ability of the surface to transfer heat to the bubble. At very high heat fluxes, near the upper limit of the nucleate boiling regime, also known as Critical Heat Flux (CHF), the situation is characterized by larger dry areas on the surface, dispersed within an interconnected network of liquid menisci. In quenching heat transfer, which refers to the rapid cooling of a very hot object by immersion in a cooler liquid, the process is initially dominated by film boiling. In film boiling a continuous vapor film completely separates the liquid phase from the solid surface; however, as the temperature gets closer to the Leidenfrost point, intermittent and short-lived liquid-solid contacts occur at discrete locations on the surface, thus creating liquid-vapor-solid interfaces once again. Ultimately, if bubble nucleation ensues at such contact points, the vapor film is disrupted and the heat transfer regime transitions from film boiling to transition boiling. Finally, in dropwise condensation, the phase transition from vapor to liquid occurs via formation of discrete droplets on the surface, and the resulting liquid-vapor-solid triple line is where heat transfer is most intense.

In all these phenomena, the triple contact line separates regions of the surface in which heat transfer is relatively poor (dry regions) from regions in which heat transfer is effective (wet regions). Any mechanistic model of the above phenomena must take into account the presence of such dry and wet regions. The specific objective of the present study is to measure the wetted area fraction (i.e. ratio of wet area to the total surface area of the heater) in pool boiling of water at atmospheric pressure, as a function of applied heat flux and liquid subcooling. Knowledge of this parameter, combined with models of other boiling parameters (such as bubble departure diameter and frequency), is key to developing a physically accurate understanding of nucleate boiling heat transfer.

2. Literature Review

Two-phase flow and heat transfer diagnostics is a rich field, which has produced several tools for probing certain aspects of the afore-mentioned phenomena. We will focus here on instruments that detect phases. For the purpose of this study, phase detectors can be divided into two broad categories: 'bulk phase detectors' and 'surface phase detectors'. The bulk phase detectors detect phases within the bulk of the flow, away from the solid surface; they include conductivity and optical probes [Kim et al. 2000, Barrau et al. 1999] and wire-mesh probes [Prasser et al. 1998]. They are intrusive instruments and generally have low (discrete) spatial resolution. On the other hand, X-ray and γ-ray tomography is non-intrusive, but rather costly/cumbersome as the radiation source has to be rotated at high speed around the test section, which also may limit the time and/or space resolution of the technique; ultra-fast approaches have been developed to increase the time and space resolution in recent years [Hori et al. 2000, Bieberle et al. 2009]. More suitable for detection of the triple contact line are the surface phase detectors. These include high-speed video, whose usefulness typically is limited by poor optical access to the

surface due to the interference from rising bubbles, and total reflection, which is rather simple and effective, but requires a heater that is completely transparent to visible light, e.g., an indium-tin-oxide film on sapphire or borosilicate glass substrate [Nishio and Tanaka 2004].

In this paper we demonstrate a recently-developed experimental technique, named DEPIcT or DEtection of Phase by Infrared Thermography [Kim and Buongiorno 2011], which is suitable for non-intrusive, high-resolution detection of the triple contact line and wet and dry areas on a boiling surface. The technique is briefly described in Section 3.

3. Description of the DEPIcT technique

DEPIcT exploits temperature differences to detect the liquid-vapor-solid triple contact line. An IR camera is used to detect the phases present on a heated surface. The key feature of this technique is to use a heater material that is IR transparent (e.g. optical grade silicon wafer), and a fluid that has a very high IR absorptivity (e.g. water). The IR camera is placed below the heater, while the fluid lies on top (Fig. 1(a)). Where the heater surface is wet, the IR camera measures the temperature of the hot water in contact with the heater. On the other hand, where vapor (whose IR absorptivity is very low) is in contact with the heater, the IR light comes from the cooler water beyond the vapor. The resulting IR image appears dark (cold) in dry spots and bright (hot) in wetted area, as illustrated in Fig. 1(b). Using the contrast between the dark and bright areas, we can visualize the distribution of the liquid and gas phases in contact with the heater surface, and thus identify the liquid-vapor-solid contact line. In other words, we measure temperature *beyond* the surface to detect phases *on* the surface. This approach distinguishes DEPIcT from the now-established IR thermometry technique with IR-opaque heaters

[Theofanous et al. 2002, Wagner and Stephan 2009, Gerardi et al. 2010, Kim et al. 2012], where the temperature measured is the temperature of the surface, which makes it hard to identify phases on the surface conclusively.

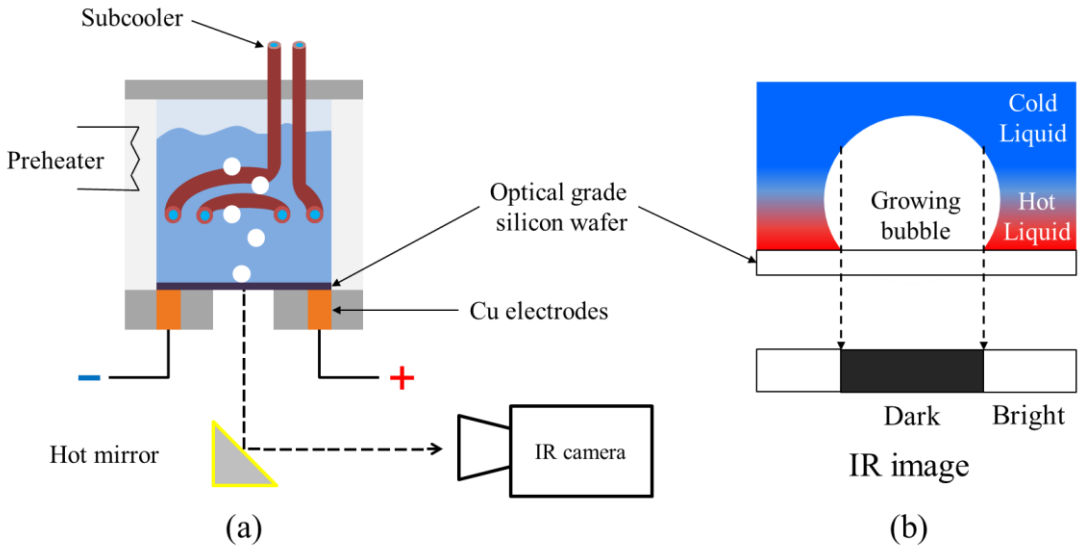

Figure 1. Experimental apparatus (a) and measurement principle (b) for the DEPIcT technique.

A complete description of DEPIcT, including an assessment of its uncertainties is reported in [Kim and Buongiorno 2011]; however, it is useful to repeat some key results here. Since DEPIcT uses a temperature measurement to detect the triple contact line, the uncertainties and sensitivities involved in the IR temperature measurement per se and the subsequent identification of the triple contact line from the IR image have to be carefully quantified. First, the IR camera used in this study (SC6000, FLIR Systems Inc., with an IR wavelength range of 3-5 μm) has a temperature resolution of 0.025°C, a maximum frame rate of 125 fps at full spatial resolution of 640×512 pixels and higher frame rates at a subset of the total image, i.e. 1000 fps at 144×144

pixels. The actual spatial resolution depends obviously on the physical size of the object being imaged. For example, if we are interested in imaging an area of 1 cm^2 and use 100×100 pixels, the spatial resolution is 100 μm. To quantify the uncertainties and sensitivities of the triple-contact-line detection, a series of tests was conducted with static droplets at various temperatures in front of background water at fixed temperature. The background water was kept at room temperature (24.3°C), while the temperature of the wafer and the droplet on it were varied from 25.6 to 30°C. Figure 2 shows the measured IR intensity (counts) of the dry and wet regions of the wafer surface for different temperatures of the droplet-wafer system. It can be seen that, although the wafer and droplet are at the same temperature, their signals are very different; this is due to the differences in the temperature of the droplet over the wafer and the background water, and makes it possible to distinguish dry surface from wet surface quite clearly. Figure 3 shows the IR intensity profile near the edge of droplets at various temperatures. If we assume the inflection point in the curves to be the nominal location of the triple contact line, the range over which the IR intensity changes significantly (~50%) is about 100 μm. Therefore, the triple contact line on the surface can be identified within 100 μm. Finally, note that the IR intensity change across the contact line is rather sharp even when the temperature difference between the wafer-droplet system and the background becomes as low as 1.3°C (=25.6-24.3).

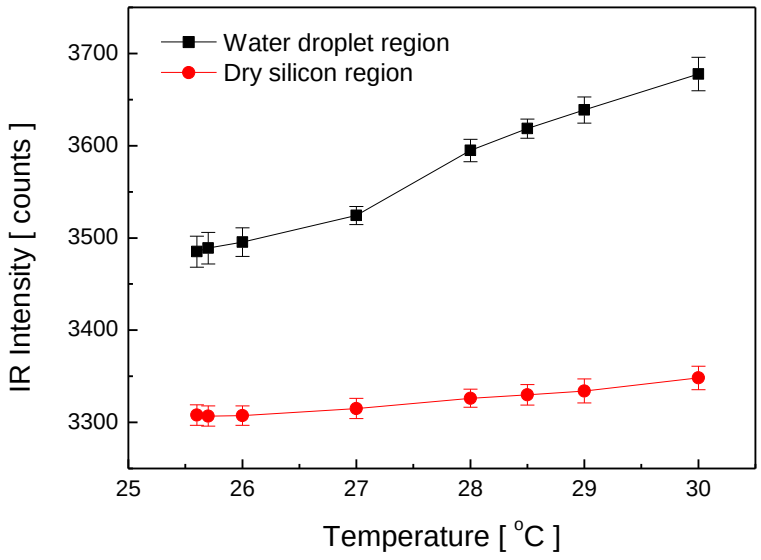

Figure 2. IR intensity emitted by a droplet and wafer at various temperatures in the uncertainty quantification tests for DEPIcT.

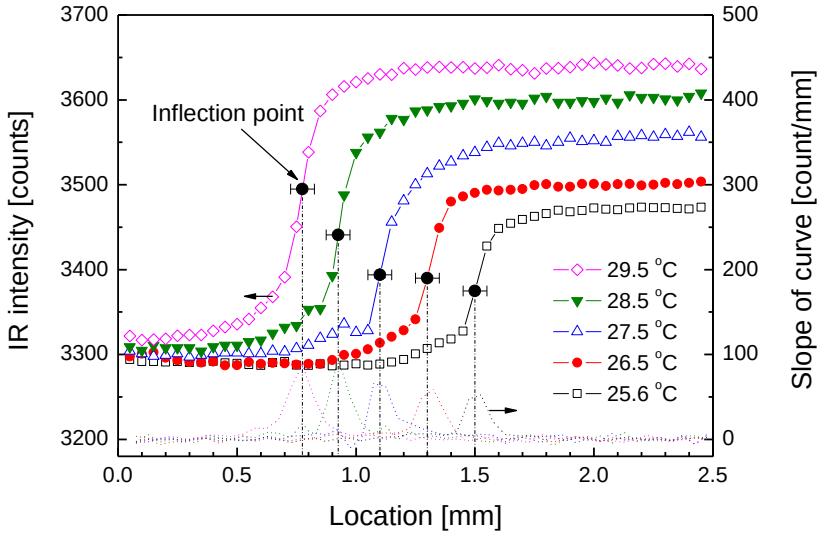

Figure 3. 1D IR intensity profile at the droplet contact line for various droplet-wafer temperatures (T_{room}=24.3°C for all cases) in the uncertainty quantification tests for DEPIcT.

Optical grade silicon wafer with the following properties was used as the heater: <100> orientation, P/Boron-doped, electrical resistivity 5-25 Ω-cm, thickness 380±25 μm, and double side polished. The relatively high electrical conductivity of this doped silicon made it possible to use direct (Joule) heating in boiling experiments. The silicon wafer heater is completely opaque to visible light, but transparent to IR, with a transmissivity of ~55% in the wavelength range of interest.

A simple experiment with a sliding droplet was conducted first, to verify the optical properties of the wafer and demonstrate the technique (Fig. 4). The liquid was pre-heated to ~30°C, while the wafer and background were at room temperature (~24°C); as a result, in the IR video the sliding droplet appears brighter than the background, and thus easily distinguishable. Comparison of high-speed video taken from above the wafer with IR video taken *through* the wafer clearly shows that the DEPIcT technique precisely and sharply captures the dynamics of liquid flow on the surface of the wafer, including the triple contact line.

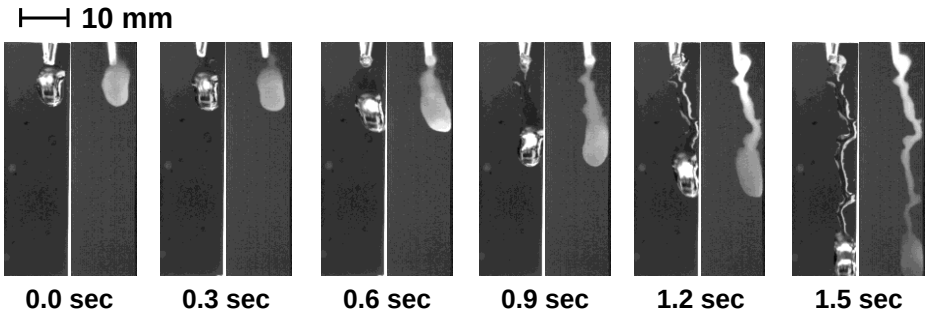

Figure 4. Droplet sliding on a vertical silicon wafer. Comparison of the high-speed video (left) and IR (right) images taken from the front and back of the wafer, respectively. The sharpness of the IR image through the wafer confirms that the wafer is essentially transparent to IR.

4. Wetted Area Fraction in Nucleate Boiling

For the nucleate boiling experiments with water at atmospheric pressure, the doped silicon wafer was accommodated into a 50×50 mm^2 square silicon substrate with Au/Cr metal pads for electrical connection to a 250-V 30-A DC power supply. The substrate had a 14×9 mm^2 opening at the center to allow for imaging by the IR camera underneath. Boiling occurred on the top face of the heater (Fig. 1). The boiling chamber was a glass cylinder of 50-mm outer diameter and 50-mm length, attached and sealed to the top face of the wafer. The water subcooling in the chamber was controlled by varying the flow rate and temperature of chilled water flowing through the subcooler tube.

The experimental procedure consisted in loading the apparatus with water, degassing it by pre-boiling the working fluid for approximately two hours using the preheater, establish the desired subcooling, and then increase the applied heat flux in small steps, with sufficient time in between steps (>1 minute) to allow for achieving a new steady state. At each heat flux step, DEPIcT was used to visualize the phase distribution on the surface at a frame rate of 500 fps. The heat flux was increased, for fixed subcooling, until the eventual occurrence of CHF destroyed the heater and terminated the test. The values of the experimentally determined CHF ranged from ~1100 kW/m^2 at saturated conditions (i.e. zero subcooling) to ~5000 kW/m^2 at high subcooling (i.e. ΔT_{sub}=50°C). The CHF data, normalized to the saturated CHF value, are shown in Fig. 5. The CHF increases with increasing subcooling, as expected from theory and various correlations, also shown in Fig. 5.

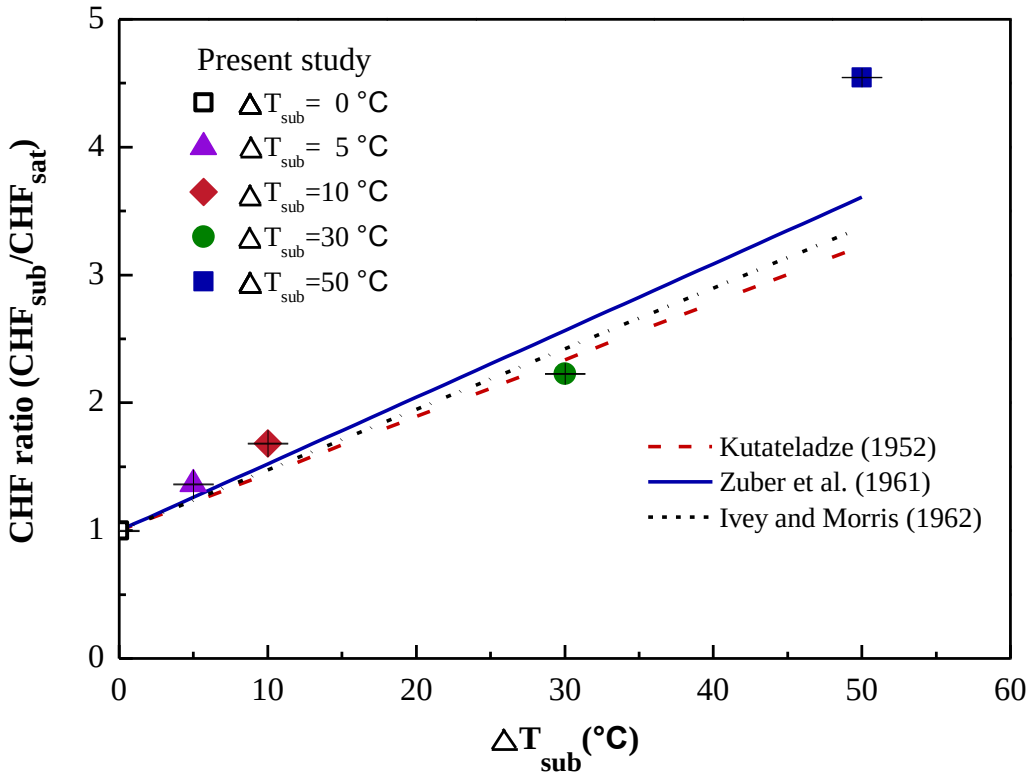

Figure 5. CHF vs subcooling for water at atmospheric pressure, boiling on horizontal silicon wafers. Error bars representing the measurement uncertainty are included, albeit small.

Of greater interest here are the DEPIcT data. It has been recently proposed that nucleate boiling heat transfer at relatively high heat flux is characterized by large dry patches dispersed within an interconnected network of liquid menisci [Theofanous and Dinh 2006]. The geometry of the liquid-vapor-solid triple contact line is highly irregular and dynamic; that is, the liquid menisci advance into and retreat from the dry patches as a function of time, due to the effects of bubble nucleation, liquid inertia (sloshing), capillary forces (surface tension) and recoil forces (evaporation). Theofanous and Dinh [2006] refer to this physical situation as the 'micro-hydrodynamics' of boiling. DEPIcT captures the micro-hydrodynamics very clearly, as shown

by the snapshot sequence in Fig. 6 for heat flux 1000 kW/m^2 and 0°C subcooling. Note that large areas of the heater surface appear dry (black) and stay dry for long periods of time (order of 30 ms), though at this heat flux we are still well below CHF, which occurred at ~1100 kW/m^2 in this particular run. All dry areas are eventually rewetted at heat fluxes below CHF. In their boiling experiments with ethanol and refrigerants, Nishio and Tanaka [2004] and Chung and No [2003] also observed large dry areas similar to ours.

A series of representative snapshots from tests at various heat fluxes and subcoolings is shown in Fig. 7. Post-processing of the DEPIcT images allows quantification of the wetted area fraction (again defined as the ratio of the wet area to the total surface area), as shown in Fig. 8. Note that relatively large instantaneous fluctuations (up to ~30% in amplitude in some cases) occur, but they do so about a stable average value, which of course depends on the heat flux and subcooling. The time-averaged wetted area fraction values are plotted in Fig. 9. It can be seen that the wetted area fraction decreases with increasing heat flux and decreasing subcooling; both trends are expected, as the ability of the liquid to stay in contact with the surface is obviously higher at lower heat flux and higher subcooling.

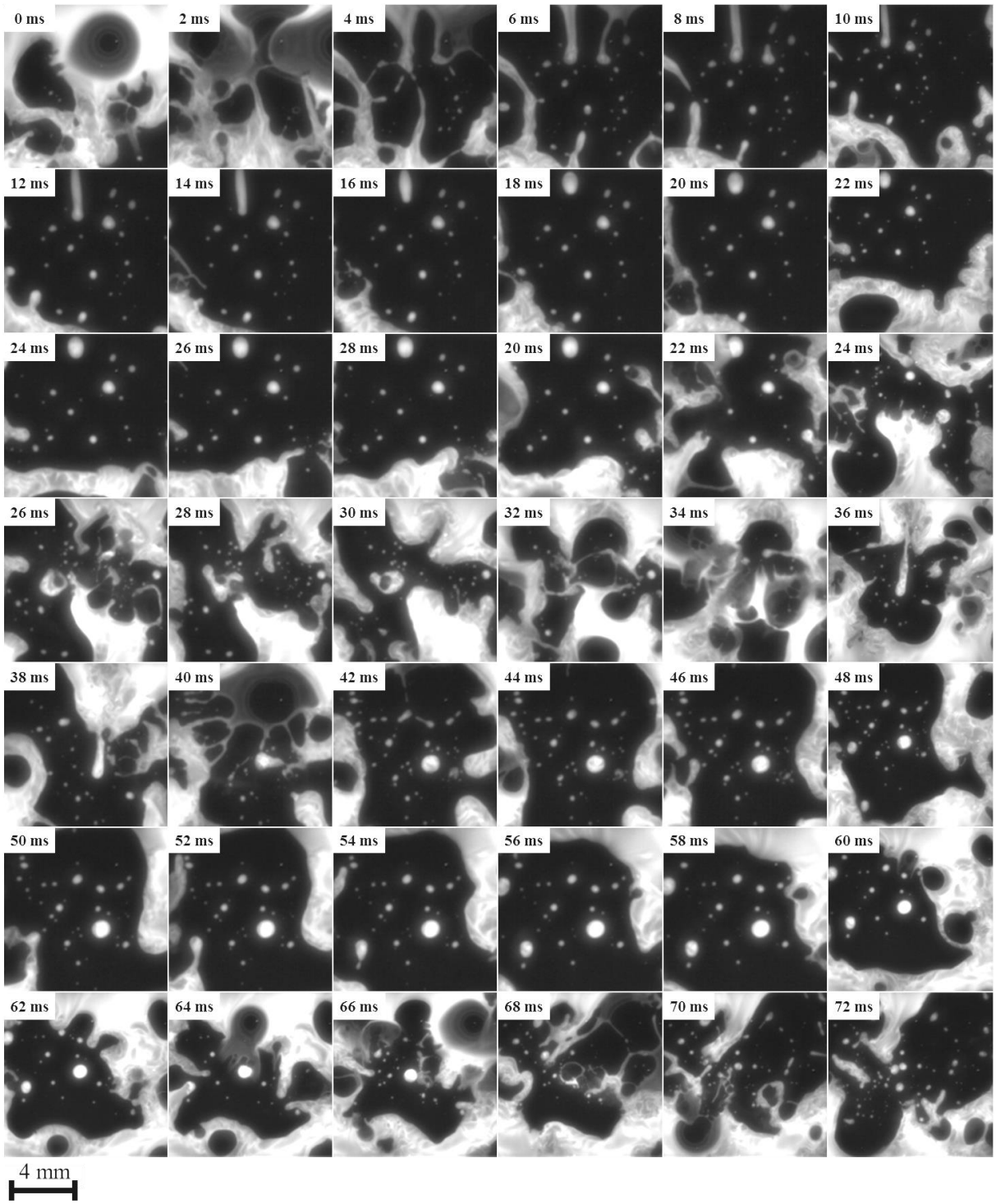

Figure 6. Time sequence of DEPIcT snapshots for water boiling at 1000 kW/m^2, 0°C subcooling and atmospheric pressure.

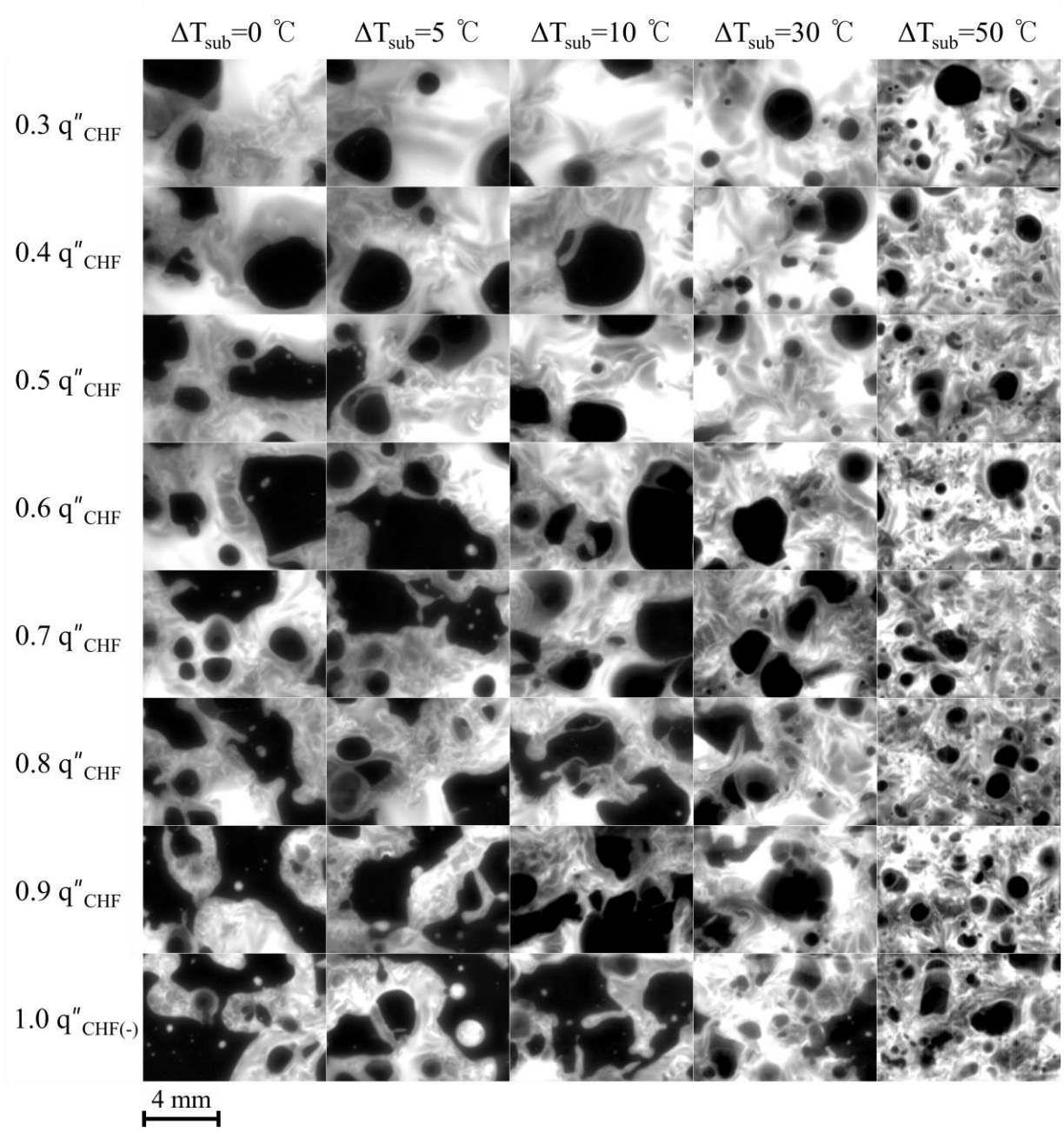

Figure 7. DEPIcT images of the boiling surface at various values of heat flux (normalized to CHF) and subcoolings. Black represents dry regions, grey and white represent wet regions. Note that the subscript 'CHF(-)' indicates the last heat flux step before CHF occurs.

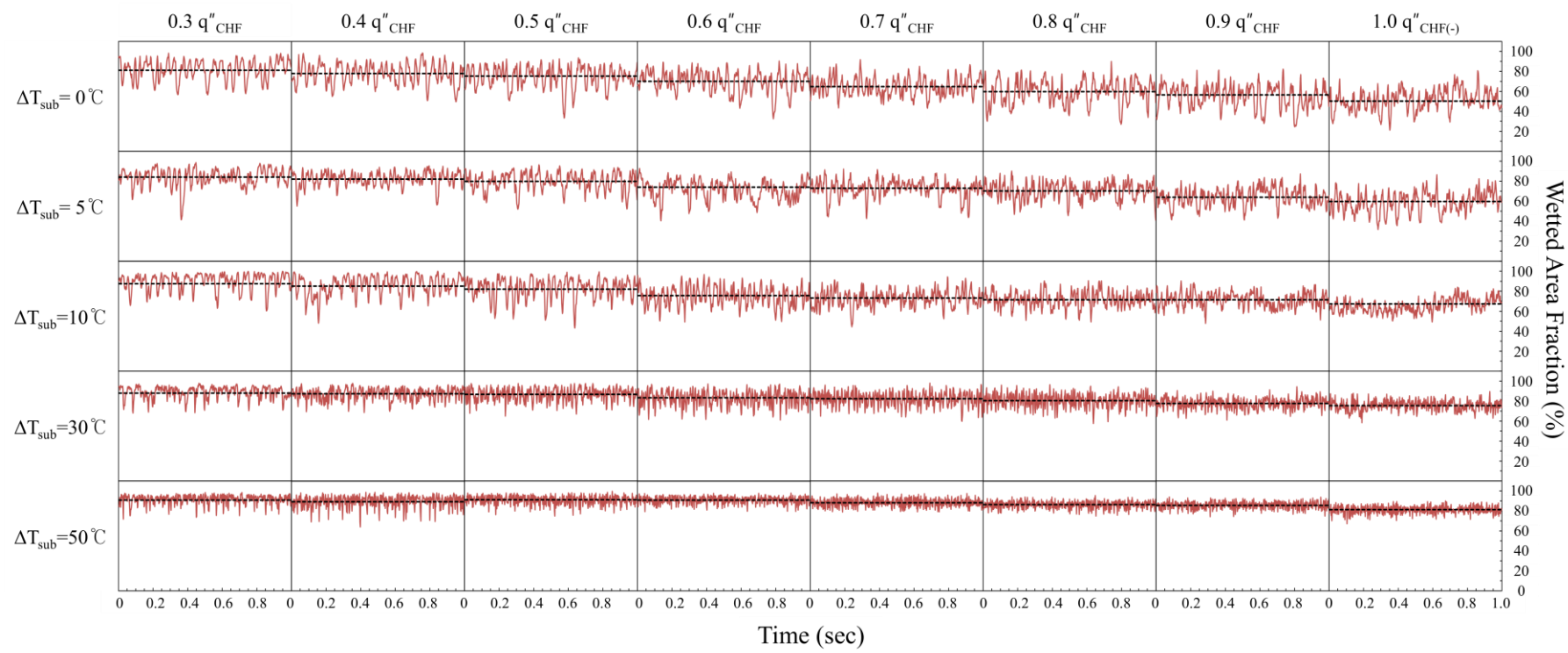

Figure 8. Instantaneous values of the wetted area fraction as a function of heat flux and subcooling. Note that the magnitude of the fluctuations decreases with increasing subcooling, for a given (normalized) heat flux. The subscript 'CHF(-)' indicates the last heat flux step before the occurrence of CHF.

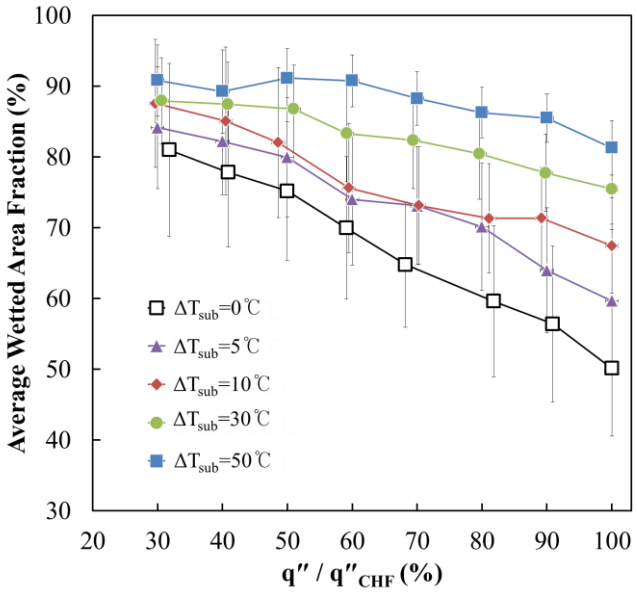

Figure 9. Time-averaged wetted fraction as a function of normalized heat flux and subcooling for water boiling over horizontal silicon heaters at atmospheric pressure.

Post-processing of the DEPIcT images also allows quantification of the triple contact line density, i.e. the length of triple contact line per unit surface area of the heater. This parameter is important because for a given value of the wetted area fraction, a higher contact line density indicates (i) a smaller average size of the dry areas (thus easier to rewet), and (ii) a higher heat transfer coefficient on average, since the triple contact line is where the local heat flux would be highest. The measured contact line density is shown in Figures 10a and 10b. It can be seen that the triple contact line density increases with heat flux for all values of the subcooling. This trend is expected, as more dry patches (and thus more contact line) appear when the heat flux increases. However, the observed relation between contact line density and subcooling is not monotonic, as can be seen in Fig. 10a and especially in Fig. 10b, where the heat flux has been normalized to the CHF. For a given value of the heat flux, there are two conflicting effects: (i) the higher subcooling cases have higher wetted area fraction, this would tend to give a lower

contact line density; but (ii) they also have individual dry patches that are on average of smaller size, which tends to give a higher contact line density. . The latter effect implies that, for a given wetted area fraction, the higher subcooling cases have a higher contact line density, which is confirmed by the plot in Figure 11.

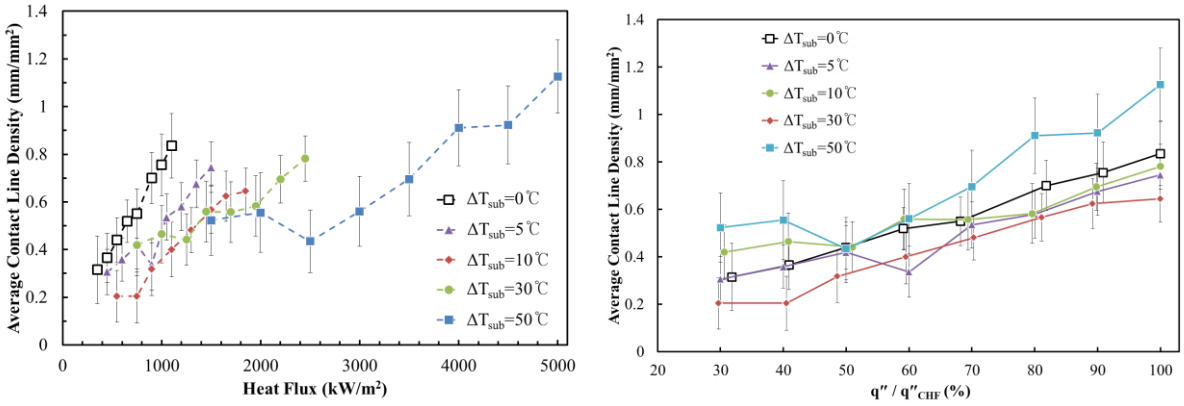

(a) (b)

Figure 10. Time-averaged contact line density as a function of heat flux (a) and normalized heat flux (b) for various subcoolings.

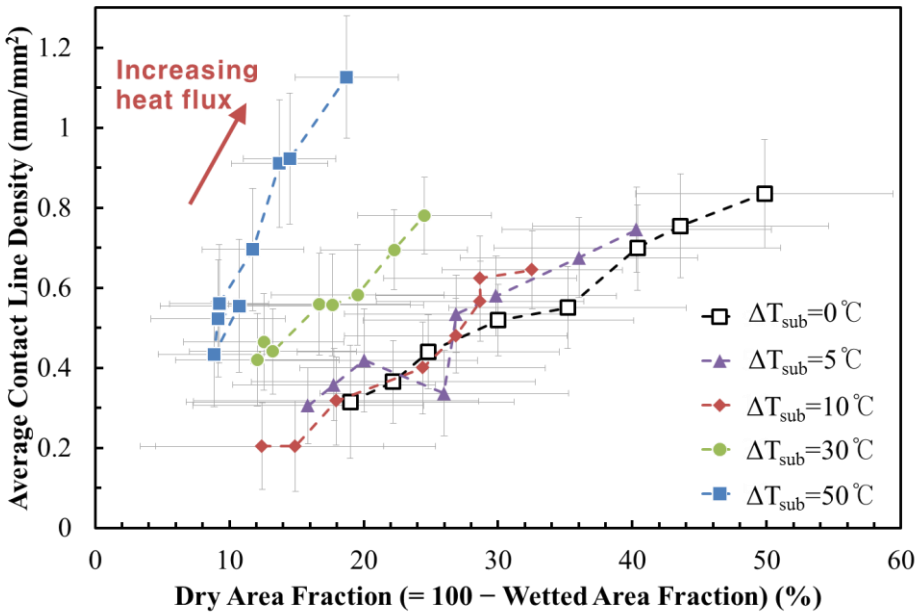

Figure 11. Contact line density vs. dry (or wetted) area fraction as a function of

subcooling for water boiling over horizontal silicon heaters at atmospheric pressure.

5. Discussion

The dynamics of the dry patches is quite interesting. Due to liquid sloshing, no point on the surface is permanently dry at any heat flux lower than CHF. Using the IR images, we estimated that at $q=1.0q_{CHF(-)}$ and $\Delta T_{sub}=0°C$ the average dry time for any given point on the surface is ~30 ms, with peaks as long as ~60 ms. Then the localized temperature rise of the silicon wafer during a dry period can be estimated as $\Delta T \sim q\, t_{dry}/(\rho\, \delta\, c)$, where t_{dry} is the dry time, and ρ, c and δ are the silicon wafer density, specific heat and thickness, respectively. ΔT ranges from 40 to 70°C. The resulting surface temperatures are well below the Leidenfrost point of the silicon wafer (>200°C), so it makes sense that the liquid can rewet the surface after a dry period. Clearly, little liquid may go a long way in keeping the surface from burning out. The data of Chung and No [9] are qualitatively similar to ours, in spite of the differences in fluid and heater materials.

At CHF the dry patches become irreversible. Fig. 12 shows that all liquid is basically gone between 4.6 s and 5.3 s after the last heat flux step increase for the $\Delta T_{sub}=0°C$ test. Before CHF occurs, the wetted fraction has large instantaneous fluctuations, but is basically stable at around 0.5. When CHF occurs, the wetted area fraction drops to ~0.01 in less than a second. Similarly, the contact line density decreases rapidly at CHF, as shown in Fig. 13. Finally, Table 1 reports the duration of the wetted area fraction transient at CHF: the surface becomes completely dry in less than a second at all values of subcoolings; however, the duration is shorter at higher subcooling. This is due to the much higher value of the CHF at higher subcooling (see

Fig. 5), i.e. when CHF finally occurs, it is a more rapid and violent phenomenon than at low subcooling. We expect these trends to hold qualitatively regardless of the surface material and fluids; however, the actual duration of the CHF transition will depend on the fluid, its pressure, the physical-chemical characteristics of the surface (in particular its wettability) and also the thermal diffusivity and thickness of the heater.

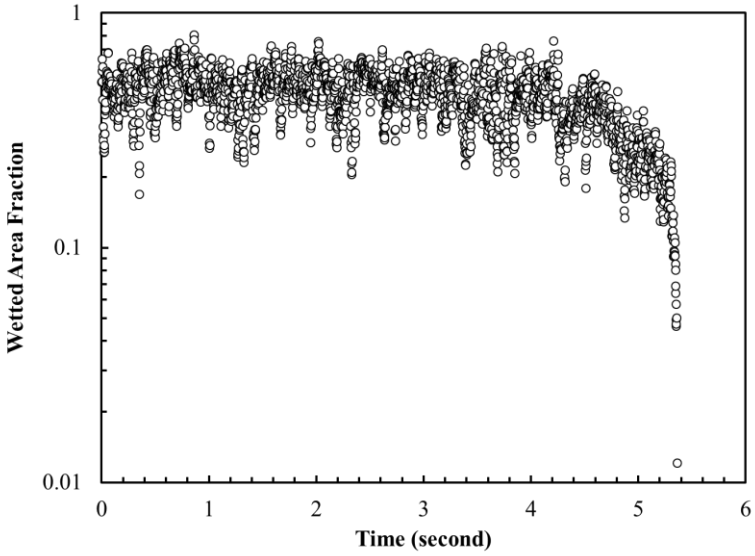

Figure 12. Time history of the wetted area fraction at CHF (~1100 kW/m^2) at ΔT_{sub}=0°C emphasizes the transition from nucleate boiling to film boiling as the wetted area fraction drops to essentially zero. .

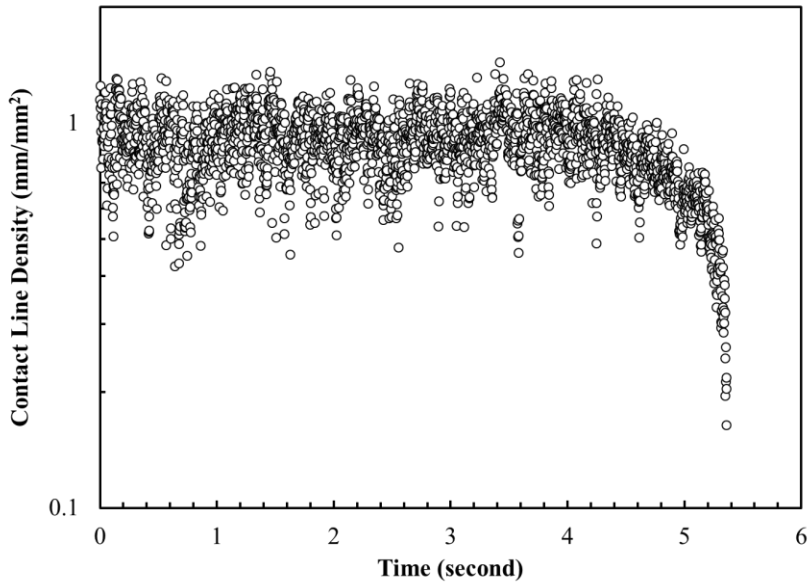

Figure 13. Time history of the contact line density during CHF (~1100 kW/m^2) at ΔT_{sub}=0°C.

Table 1. Time required for the transition from nucleate boiling to film boiling.

ΔT_{sub}	0°C	5°C	10°C	30°C	50°C
Δt	~0.7 sec	~0.7 sec	~0.6 sec	~0.4 sec	~0.3 sec

6. Conclusions and Future Work

DEPIcT, a new high-speed phase detection technique uniquely suitable for two-phase heat transfer studies, was applied to measurement of the wetted area fraction in pool nucleate boiling of water at atmospheric pressure over smooth silicon wafers. The data can be summarized as follows:

- CHF increases with increasing subcooling.

- The wetted area fraction monotonically decreases with increasing heat flux and decreasing subcooling.
- At any given heat flux and subcooling there is a significant fraction of the boiling surface that is dry, albeit reversibly. That is, each point on the surface is periodically rewetted by liquid sloshing over the surface.
- The dry patches become irreversible at CHF, when the wetted area fraction drops to essentially zero over a period of <1 second.
- The duration of the CHF transient is lower for higher subcooling.
- The contact line density (i.e. triple contact line length per unit area of the boiling surface) was also measured and found to increase with increasing heat flux (for a given subcooling) and increasing subcooling (for given wetted area fraction).

Future work that would be relevant to nuclear reactor applications includes studying how the wetted area fraction and contact line density depends on water pressure, velocity (effect of flow boiling) and surface characteristics, in particular surface wettability (contact angle), surface roughness and the presence of interconnected porosity on the surface, such as CRUD deposits. Also, it would be interesting to correlate the wetted area fraction and contact line density data to the overall and local heat transfer coefficient on the surface; it is expected that higher wetted area fraction and contact line density would result in higher values of the heat transfer coefficient. Unfortunately DEPIcT only detects surface phase, but not surface temperature simultaneously, so measurement of the heat transfer coefficient was not possible in this study. Work in our group is underway to extend DEPIcT to simultaneous measurement of surface temperature and surface phase.

Acknowledgements

This work has been made possible by a Seed Fund grant from the MIT Energy Initiative, and was supported by National R&D Program through the National Research Foundation of Korea (NRF) funded by the Ministry of Education, Science and Technology (2012M2B2A9A02029577). Prof. Karl Berggren and Dr. Sebastian Strobel of MIT are acknowledged for providing the silicon wafers used in this study. Thanks to Dr. Truc-Nam Dinh of the Idaho National Laboratory (INL) for providing useful comments on the work.

References

- Barrau, E., Rivière, N., Poupot, Ch., Cartellier, A., 1999. Single and double optical probes in air-water two-phase flows: real time signal processing and sensor performance. Int. J. Multiphase Flow. 25(2). 229-256.
- Bieberle, M., Fischer, F., Schleicher, E., Koch, D., Menz, H-J., Mayer, H-G., Hampel, U., 2009. Experimental two-phase flow measurement using ultra fast limited-angle-type electron beam X-ray computed tomography. Experiments in Fluids. 47(3). 369-378.
- Chung, H. J., No, H. C., 2003. Simultaneous visualization of dry spots and bubbles for pool boiling of R-113 on a horizontal heater. Int. J. Heat Mass Transfer, 46. 2239–22 51.
- Gerardi, C., Buongiorno, J., Hu, L. W., McKrell, T., 2010. Study of Bubble Growth in Water Pool Boiling Through Synchronized, Infrared Thermometry and High-Speed Video. Int. J. Heat Mass Transfer. 53. 4185-4192.
- Hori, K., Fujimoto, T., Kawamishi, K., Nishikawa, H., 2000. Development of an ultrafast X-ray computed tomography scanner system: application for measurement of instantaneous void distribution of gas-liquid two-phase flow. Heat Transfer-Asian Research. 29(3). 155-65.
- Ivey, H. J., and Morris, D. J., 1962. On the relevance of the vapor-liquid exchange mechanism for subcooled boiling heat transfer at high pressure. British Repo rt AEEW-R-137. Atomic Energy Establishment. Winfrith.
- Kim, H., Buongiorno, J., 2011. Detection of Liquid-Vapor-Solid Triple Contact Line in Two-Phase Heat Transfer Phenomena Using High-Speed Infra-Red Thermometry. Int. J. Multiphase Flow. 37. 166-172.
- Kim, S., Fu, X.Y., Wang, X., Ishii, M., 2000. Development of the miniaturized four-sensor conductivity probe and the signal processing scheme. Int. J. Heat Mass Transfer. 43(22). 4101-4118.
- Kim, T.H., Kommer, E., Dessiatoun, D., Kim, J., 2012. Measurement of two-phase flow an d heat transfer parameters using infrared thermometry. Int. J. Multiphase Flow. 40. 56-67.
- Kutateladze, S. S., 1952. Heat transfer during condensation and boiling. Translated from a pu blication of the State Scientific and Technical Publishers of Literature on Machinery. Mosco

w-Leningrad. AEC-tr-3770.

- Nishio, S., Tanaka, H., 2004. Visualization of boiling structures in high-heat flux pool-boiling. Int. J. Heat Mass Transfer. 47. 4559-4568.
- Prasser, H.M., Bottger, A., Zschau, J., 1998. A new electrode-mesh tomography for gas–li quid flows. Flow Measurement and Instrumentation. 9. 111–119.
- Theofanous, T.G., Dinh, T.N., 2006. High heat flux boiling and burnout as microphysical phenomena: mounting evidence and opportunities. Multiphase Science and Technolog y. 18(3). 251-276.
- Theofanous, T.G., Tu, J.P., Dinh, A.T., Dinh, T.N., 2002. The Boiling Crisis Phenomenon. J. Experimental Thermal Fluid Science. 26(6-7). 775-792. 793-810.
- Wagner, E., Stephan, P., 2009. High-resolution measurements at nucleate boiling of pure FC-84 and FC-3284 and its binary mixtures. ASME Journal of Heat Transfer. 131(12). 121008.
- Zuber, N., Tribus, M., Westwater, J.W., 1961. The hydrodynamic crisis in pool boiling of sat urated and Subcooled liquid. Proc. Int. Heat Transfer Mtg. Boulder. Co. 27. 230.